Lab on a Chip

Accepted Manuscript

ROYAL SOCIETY OF CHEMISTRY

www.rsc.org/loc

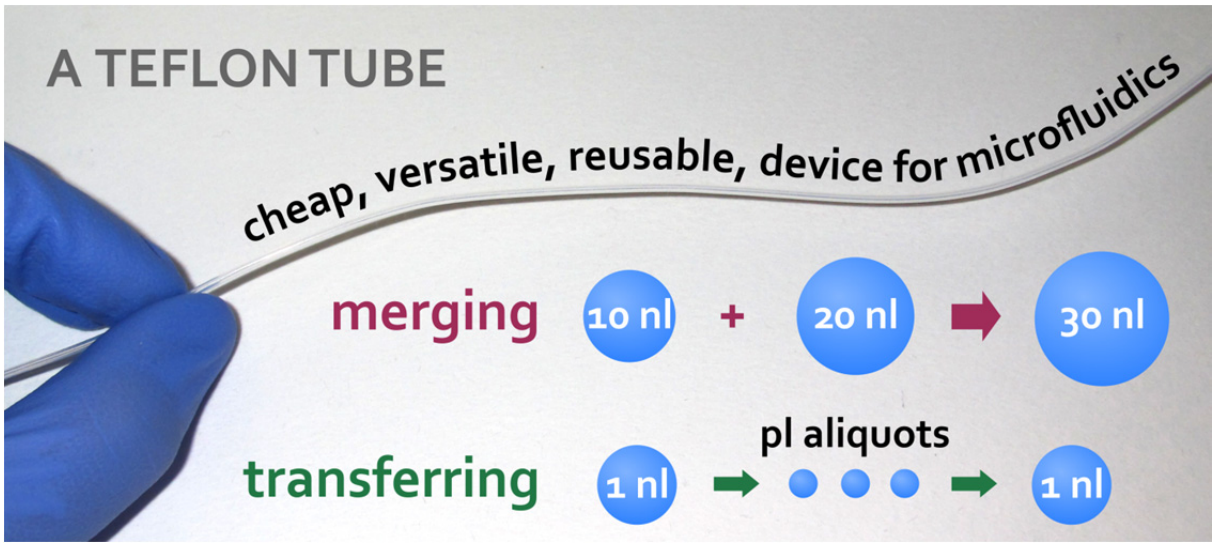

Lab on a Chip

Paper

Merging drops in a Teflon tube, and transferring fluid between them, illustrated by protein crystallization and drug screening

Received 00th January 20xx,
Accepted 00th January 20xx

DOI: 10.1039/x0xx00000x

www.rsc.org/

A. Feuerborn,[a] A. Prastowo,[b] P. R. Cook,[a] and E. Walsh[b*]

The ability to manipulate drops with small volumes has many practical applications. Current microfluidic devices generally exploit channel geometry and/or active external equipment to control drops. Here we use a Teflon tube attached to a syringe pump and exploit the properties of interfaces between three immiscible liquids to create particular fluidic architectures. We then go on to merge any number of drops (with volumes of micro- to nano-liters) at predefined points in time and space in the tube; for example, 51 drops were merged in a defined order to yield one large drop. Using a different architecture, specified amounts of fluid were transferred between 2-nl drops at specified rates; for example, 2.5 pl aliquots were transferred (at rates of ~500 fl/s) between two drops through inter-connecting nano-channels (width ~40 nm). One proof-of-principle experiment involved screening conditions required to crystallize a protein (using a concentration gradient created using such nano-channels). Another demonstrated biocompatibility; drugs were mixed with human cells grown in suspension or on surfaces, and the treated cells responded like those grown conventionally. Although most experiments were performed manually, moderate high-throughput potential was demonstrated by mixing ~1,000 different pairs of 50-nl drops in ~15 min using a robot. We suggest this reusable, low-cost, and versatile methodology could facilitate the introduction of microfluidics into workflows of many experimental laboratories.

Introduction

Droplet-based microfluidics allows manipulation of volumes down to femto-liters; it has applications in biomedicine – including single-cell diagnostics,[1-3] DNA amplification using the polymerase chain reaction (PCR)[4,5] and the synthesis of nano-materials.[6] The underlying aim in many applications is to bring together and mix different water-soluble reagents. One challenge is to deliver such reagents to drops,[7] and various approaches are available to control the coalescence of a few drops either actively (e.g., using lasers or electrodes)[8] or passively (e.g., using channel geometry).[9] For example, pico-injection has been applied to modify contents of pre-formed drops as they flow past a fixed point in a channel,[10] and to create new drops with slightly varying contents.[11,12] Drops have also been merged as they flow through a PDMS channel by exploiting interfacial tensions between two[11,13] (perhaps in association with a chemical method)[14] or three[15] immiscible liquids.

Several simplified methods for droplet merging have been proposed that do not utilise a preformed microchip. These include modular systems that allow many tubes/channels and T-junctions to be joined together easily,[16,17] and a robot-driven capillary that first "prints" arrays of drops on a hydrophilic-patterned surface and then adds additional drops to specified locations (applied to single-cell RT-PCR).[18] Whilst these methods alter drop contents in a "digital" way (i.e., by adding discrete volumes), there remains no "analogue" variant that allows continuous changes in drop content (i.e., by gradual advection into, or out of, pre-formed drops) – aside from molecular diffusion through walls/fluids[19,20] (where control is limited by the porosity of the wall to molecules of interest).

The use of multiple emulsions has a long history in microfluidics.[15,21-26] Here, we exploit three or more phases to create fluidic architectures where individual drops have an aspect ratio (length to diameter) >1, and use them to merge drops, and transfer fluid between them. The approach is simple and versatile. It exploits interfacial tensions at the boundaries between immiscible fluids contained in a Teflon tube. Flow through the tube is driven by a syringe pump (or gravity), and interfacial tension is used to bring drops together, and transfer aqueous fluids gradually between pre-formed ones through fluidic nano-channels (~40-nm wide) at rates down to fl/s. We apply the first approach to confirm biocompatibility by testing drugs for their effects on human cells, and the second to screen conditions for crystallizing a protein. We also demonstrate moderate high-throughput capability by mixing ~1,000 pairs of 50-nl drops in ~15 min

[a] Sir William Dunn School of Pathology, University of Oxford, South Parks Road, Oxford OX1 3RE, UK.
[b] Osney Thermo-Fluids Laboratory, Department of Engineering Science, University of Oxford, Osney Mead, Oxford OX2 0ES, UK. Email: edmond.walsh@eng.ox.ac.uk; Fax: +44 1865 288756; Tel: +44 1865 288731
Electronic Supplementary Information (ESI) available: [Supplementary methods, Figs S1-S6, Table S1, Movies S1-S5]. See DOI: 10.1039/x0xx00000x

using a robot. We anticipate the general approach will prove useful in handling and manipulating small volumes.

Methodology

Our approach utilizes at least three immiscible fluids, and different ones are used for different experiments. Interfaces between three such fluids are in equilibrium when the "Neumann triangle" is satisfied (as in Fig. 1Ai – where phase 1 is FC40 plus surfactant, phase 2 is water containing a red dye, and phase 3 is silicone oil). Then, the interfacial tension, γ, between any two fluids is less than the combination of interfacial tensions between the others ($\gamma_{1-2} < \gamma_{1-3} + \gamma_{2-3}$).[27,28] However, drops-within-drops form if conditions no longer satisfy the Neumann triangle and $\gamma_{1-2} > \gamma_{1-3} + \gamma_{2-3}$ (which is achieved in this case by removing surfactant from phase 1). Now, fluid 3 forms the interface between fluids 1 and 2, so fluid 1 engulfs 3, and 3 engulfs 2 (Fig. 1Aii). The volumes of the immiscible drops are independent of the inequality that leads to engulfment, which is sometimes recast as a spreading coefficient.[29] In most cases, surfactants (amphiphiles) are added to phase 3 to increase the inequality and so stabilize the chosen fluidic architecture. In all cases, the fluorocarbon "wets" the Teflon to create a continuous and protective film along the tube wall, so water-soluble molecules are unlikely ever to touch (or adhere to) the wall.

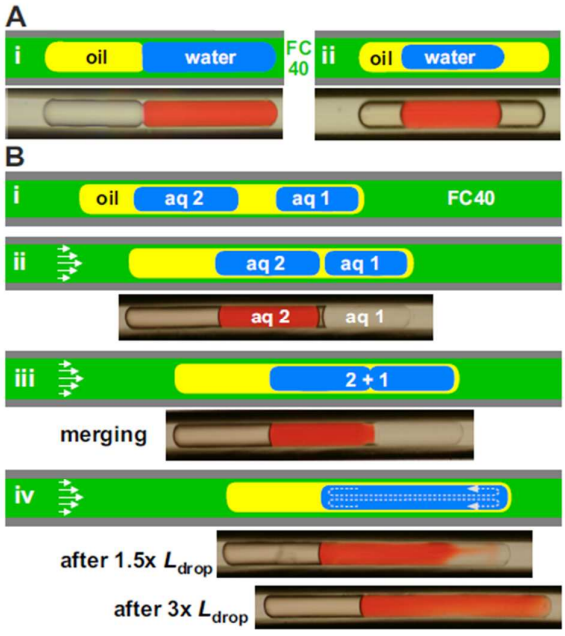

Figure 1. Drop merging and mixing (150-μm tubes). Schematics illustrate structures seen in movie frames below (some water drops contain red dye). (A) Structures depend on interfacial tension. (i) All three fluids are stably in contact (fluids – FC40 + 10% PFO, water + dye, 5-cSt silicone oil). (ii) If PFO is omitted, FC40 engulfs the oil, which engulfs water + dye. (B) Merging drops during flow (fluids – FC40, water ± dye, tetradecane + 1% Span80). (i) An oil drop engulfs two 10-nl aqueous drops. (ii) During flow (arrows illustrate parabolic velocity profile), relative velocities are: water drops > oil super-drop > bulk FC40. Then, as water-drop 1 cannot travel faster than the front of the oil super-drop, drop 2 soon catches it up. (iii) Drop 2 merges with 1. (iv) Vortices (curved arrows) mix contents (distance travelled indicated in drop lengths, L_{drop}).

We now illustrate the principle we will use to merge aqueous drops, beginning with a simple case involving a train of two drops (~10 nl) engulfed in one oil super-drop (~10 nl; Fig. 1Bi; Movie S1; all movies shown run in real time). Starting the pump connected to the tube causes laminar flow. Then drops closer to the centre-line move at a higher speed than the engulfing fluid, and the relative mean velocities of fluids are: water > oil > FC40. Water-drop 1 is constrained from moving faster than the surrounding oil by the oil/FC40 interface. However, drop 2 is unconstrained and moves faster, and so catches up drop 1 (Fig. 1Bi,ii). The two drops merge as soon as they touch because the interface is unstable (Fig. 1Biii). Subsequently, vortices mix contents within ~4 drop lengths (Fig. 1Biv). Such "front-to-back" mixing is efficient, unlike the "side-by-side" mixing found in some microfluidic devices.[30]

Materials and methods

General reagents and equipment

FC40 and HFE7500 were from Acota, Abil®EM180 surfactant from Surfachem, and all other fluids from Sigma Aldrich unless otherwise stated. Where indicated, aqueous drops contained water-soluble dyes: 5 mg/ml Allura Red, 2 mg/ml toluidine blue, 6 mg/ml haematein (yellow), or 200 μM carboxy-fluorescein unless otherwise stated. Surfactant concentrations are given on a weight-to-weight basis. Teflon (poly-tetrafluoroethylene, PTFE) tubing (50-620 μm bore; Cole-Parmer/Zeus) was attached to a programmable syringe pump (Harvard PhD Ultra I/W) fitted with Hamilton air-tight glass syringes – with sizes ranging from 5 μl to 2.5 ml (Hamilton 800/1700 and 1000 series) – and blunt needles of appropriate gauge (i.e., 20-32). In some cases, bipartite tubes with thin and thick segments were used for high-throughput analyses. Then, the smaller segment allows manipulation of smaller volumes, whilst the larger one reduces the pressure drop (and so the possibility of leaks), minimizes the tube length required to store merged drops during multiplexing (as trains become shorter in the wider tube), and allows the use of lower-cost optics for detection of fluorescence/colour (as drops have a larger depth due to increased diameter). Conditions used for individual experiments are described in Electronic Supplementary Information.

Interfacial tension measurement

Interfacial tensions were measured using the pendant-drop technique and a commercial system (First Ten Angstroms 1000). Drops were ejected from 16-30 gauge stainless-steel blunt needles (using a Harvard syringe pump or a Gilmont micro-meter syringe) into the less-dense fluid in a 2-ml cuvette. The manufacturer's software was used to calculate the interfacial tension for each image. Before using any new fluids, the system was calibrated; the interfacial tension of filtered water/air or FC40/air was measured and good agreement was found with established values of 72 and 16 mN/m.

Static and dynamic interfacial tension

During flow, internal circulation in drops[31] can transport surfactant molecules from the front to the back of a drop along the interface. Hence, it will be the dynamic interfacial tension that should be used when determining the Neumann inequality. Unfortunately the dynamic interfacial tension is both difficult to measure directly, and varies – as we will demonstrate. Therefore, we select fluids for the fluidic architecture that give a strong Neumann inequality based on static interfacial tensions. Estimates of this inequality (using data in the literature)[32] demonstrate that this is easily achievable for most fluid combinations. For example, the equilibrium interfacial tension between fluorocarbon and water is ~45 mN/m, between fluorocarbon and oils is ~8 mN/m, and separating oil + surfactant and water is ~15 mN/m. The result is a strong inequality, so that fluorocarbon engulfs oil, and oil engulfs water (i.e., 45 > 15+8). This architecture is used for merging. When using surfactant-free fluids, the static interfacial tension is expected to be equal to the dynamic one, so that interfacial tensions from the pendant-drop method can be applied more definitively to the flowing system.

Generation of arrays of drops

Carrier fluids (FC40, HFE7500, or FC40 + HFE7500, all ± surfactant), aqueous fluids (± additive), and separating fluids (tetradecane, dodecane, 5-cSt silicone oil, silicone oil AR20, sunflower oil, all ± surfactant) – which are called "oils" in the main text – were generally placed in separate wells of a 96-well plate. To avoid the need to overlay reagents with oil, drops were created by operating the syringe pump attached to a PTFE tube. Initially, the tube, syringe, and needles were all filled with FC40/HFE7500 ensuring no gas was present. The syringe pump was programmed to operate in "withdraw/stop mode". In withdrawal mode, the tip of the tube was immersed manually in the fluid until the required amount was loaded (flow rates 0.01-2 ml/h); then the pump was stopped, the tip moved to the next fluid, and withdrawal mode restarted. This sequence was repeated to produce the required fluidic architecture.

A "train" containing one aqueous drop engulfed in one oil "super-drop" can be prepared by filling a Teflon tube attached to the programmable pump with fluorocarbon, and dipping the tip of the tube successively into water and oil. Use of the custom "withdraw/stop" program provides precise control over drop sizes as fluids are loaded during "withdraw", and the tip is transferred to a new fluid during "stop". This program utilizes the software built in to the syringe pump to specify how long the "withdraw" and "stop" modes last. More aqueous drops can be engulfed in one oil super-drop by including extra dips into water and oil before the last into fluorocarbon (Fig. 1B, Fig. S1). Fluidic architectures are stably maintained when flow stops/restarts. Additional independent trains (separated by fluorocarbon) are prepared by repeating this simple process. As we shall see, each train then becomes an independent reaction vessel that utilizes only reagents in that train.

When loading tubes, aqueous reagents were initially covered with separating fluid to reduce the possibility of ingesting air into tubes, which then complicates flow patterns as pumps start and stop (due to the compressibility of the air). However, the oil overlay was found to be unnecessary if tubes and syringes were originally filled with degassed fluorocarbon without air drops, and if no cavitation occurred when flow stopped and started. Consequently, use of a low-viscosity carrier was preferred as it reduced the pressure drop and enabled faster flow rates. Therefore, HFE7500 was often used, but it was replaced with FC40 to produce particular fluidic architectures and provide greater biocompatibility. Use of smaller syringes and larger-bore tubes also reduced the probability of air ingestion. For example, use of a 250-μl gas-tight syringe (Hamilton) connected to 350-μm diameter tube via a blunt needle led to no air ingestion, but a 2.5-ml syringe connected to the same tubing resulted in sporadic ingestion. For tube diameters between 100-200 μm, we used 50-100 μl syringes, and for 50-μm tubing 5-10 μl syringes. Although the tube is filled under sub-atmospheric pressure, ends of loaded tubes can easily be capped with a resin-filled blunt needle and operated under high pressure; however, the system is not conducive with closed-loop functionality.

For Figures 4-6, S2, and S3, tubes were loaded using stepper motors. The accuracy of drop generation depends on the drop size (the longer the better) and tube wall thickness (the smaller the better). For example, 100 drops (400 nl) were loaded into a train in a 350-μm diameter tube (using a 250-μl syringe); they had a maximum variation in volume of <4%. This variation was typically found with all syringe/tube combinations used.

Although most experiments were performed by manually dipping between reservoirs in a 96-well plate, a "robot" with three axis-positioning systems (Z-400, CNC Step, Germany) is used to demonstrate automated high-throughput potential.

Measurement of drop velocity and length

Drop velocity and length were measured using two orthogonal LEDs/photodiodes spaced 1 m apart along a transparent PTFE tube (350 or 620-μm bore; photodiodes were ~0.5 m from tube ends; Fig. 2). As all fluids used in a single experiment had different refractive indices, photodiode voltage depends on the fluid in the light path. Times taken by drops to travel through one light beam and between beams were recorded, and drop length and inter-drop distance calculated using custom software, with sampling frequency of up to 500 Hz. To determine tube diameter, FC40/HFE7500 was pumped through a virgin tube at a known flow rate. The time taken for the leading FC40/HEF7500-air interface to travel between the two photodiodes was recorded, and diameter calculated using the continuity equation and known flow rate set on the syringe pump.

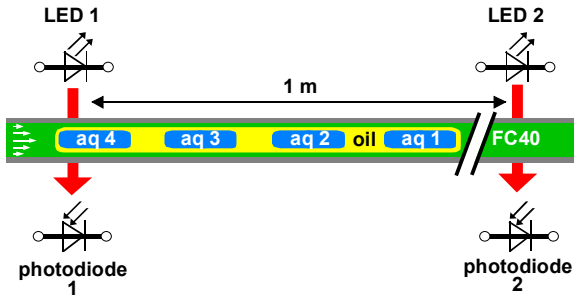

Figure 2. Experimental setup for measurement of drop length and velocity; photo-diode voltage reflects which fluid is in the light beam. Times taken by drops to travel through one light beam and between beams were recorded, and drop length and velocity calculated.

Drop velocity and film thickness

The thickness of a film engulfing a drop (as in Fig. 3) may be estimated by implementing the assumptions of an inviscid ($\mu_1 >> \mu_2$) or solid drop ($\mu_1 << \mu_2$), and applying continuity to the flow within a circular tube. For an inviscid drop, where R = channel radius, r = drop radius, h = film thickness, Q = flow rate, U = mean velocity of fluids, we obtain:

$$\dot{Q}_{mean} = \dot{Q}_{film} + \dot{Q}_{drop}$$

The velocity in the film region is modelled as zero or a linear velocity profile (Couette flow) to determine the limits of the film thickness for the cases of inviscid or solid drops respectively (Fig. 3ii). Equating flow rates at axial positions in carrier fluid (phase 1) and drop region (phase 2) yields:

$$\left[\pi R^2 U_{mean} = \pi (R-h)^2 U_{drop}\right]_{inviscid}$$

$$\left[\pi R^2 U_{mean} = \pi (R^2 - (R-h)^2)\frac{U_{drop}}{2} + \pi (R-h)^2 U_{drop}\right]_{Visc}$$

Solving these equations where $h << R$, provides

$$\left[\frac{h}{R}\right]_{\text{inviscid drop}} = \frac{1}{2}W$$

$$\left[\frac{h}{R}\right]_{\text{solid drop}} = W$$

$$W = \frac{U_{drop} - U_{mean}}{U_{drop}}$$

where W is referred to as the excess velocity. These equations, or similar, have been derived by several authors for an inviscid[33,34] and solid drop.[35] Therefore, when flow is induced in the capillary illustrated in Figure 3i, the distance between x_f and x_d reduces by Δx which depends on film thickness. The film thickness, in the limits of an inviscid or solid drop, may be estimated by measuring the velocities of the drop and carrier fluid. For all cases where $\mu_1 \sim \mu_2$, it is expected to reside between these two limits. The same equations can then be applied to our new fluidic architecture illustrated in Figure 1B, where film thickness between water and oil phases may be estimated by measuring the mean velocity of both (assuming the carrier-fluid film surrounding the oil is unchanged over the length of the oil drop). The resultant film thicknesses, from the inviscid and solid drop equations, provide the limits of film thicknesses for any viscosity ratio between water and the engulfing oil drops.

The prediction of h/R, and hence excess velocity of the engulfed drops/bubbles, has been extensively studied[28,30-36] since the original experimental[36] and theoretical works;[37] most works identify the Capillary number [$Ca = \mu V/\gamma$] as the appropriate scaling parameter in such problems.

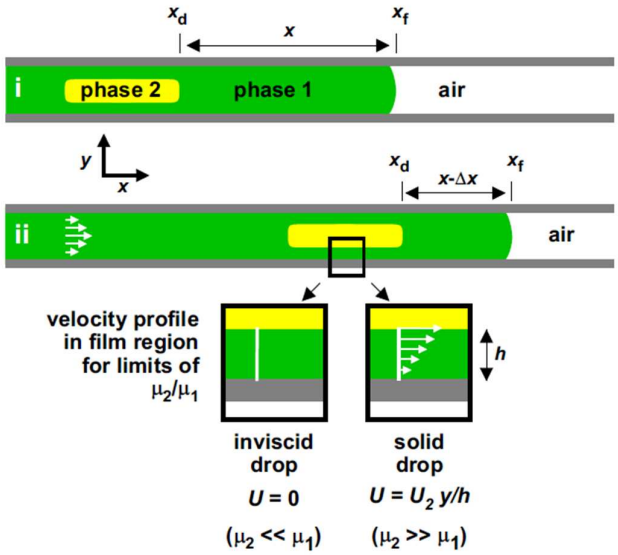

Figure 3. Schematic of immiscible fluids flowing in a circular capillary; (i) phase 2 (with leading interface at x_d) is engulfed by phase 1 (with leading interface at the air, x_f), which wets the wall. (ii) After flow, the distance between interfaces x_f and x_d has reduced due to the velocity of phase 2 (which is > phase 1). Also illustrated are the simplified velocity profiles in the film region between phase 2 and the wall, for an inviscid and solid drop.

Results and discussion

Relative drop velocities

To predict where and when two drops might merge in a train like that in Figure 1Bi, it is necessary to determine the excess velocity of drop 2 over drop 1. Sets of 10 trains containing two aqueous drops (each train as in Figure 1Bi) were created and the velocity of each drop recorded over a range of carrier-fluid velocities. The excess velocity of aqueous drops over the carrier-fluid velocity for each train is shown in Figure 4A. Across the ten trains the standard deviations range from 3-11% of the excess velocity between drops pairs (within the limits of carrier-fluid velocities of 5.5-0.46 mm/s).

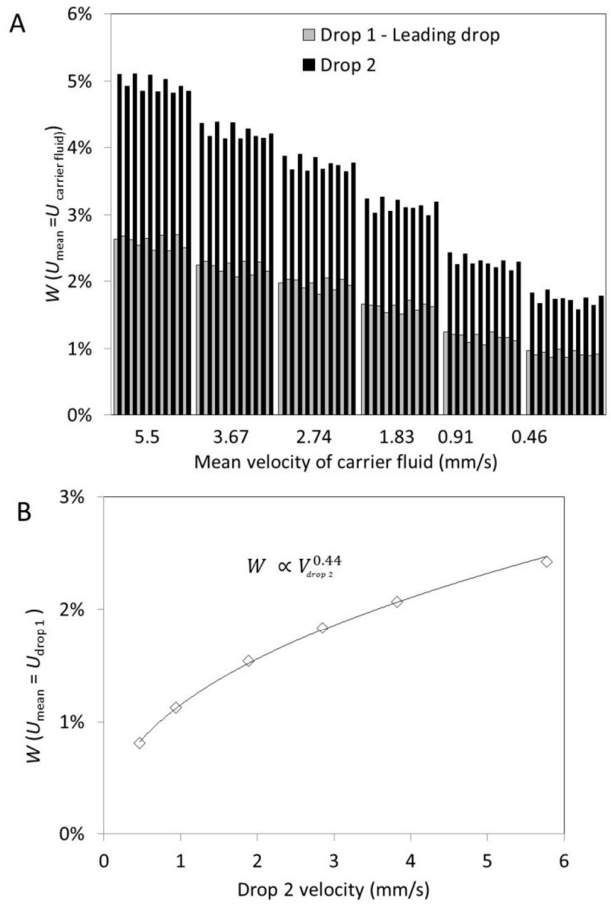

Figure 4. The effect of flow rate on the velocity excess, *W*, of each of two drops within sets of 10 trains in a 620-µm tube (fluids – FC 40, water, tetradecane + 1% Span80). Drop 1 and 2 are separated by a sufficient distance so they do not merge between photodiodes in Figure 2. (A) Velocity excess of all drops relative to velocity of carrier fluid. (B) Average excess velocity of drop 2 relative to 1 for different mean carrier-fluid velocities (diamonds, with line of best fit).

Thus, at one meter from the tube inlet in the experiment described in Figure 4, the distance between drop 1 and 2 reduces by 16 ± 1 mm (assuming an uncertainty of one standard deviation) at a carrier-fluid velocity of 1.83 mm/s. Considering a more realistic problem where the distance between drops is 2 mm at the inlet, the merge location is 128 ± 9 mm into the tube. Figure 4B shows the average excess velocity of drop 2 over 1 for various mean carrier-fluid velocities. The best-fit power law shows that $W \propto V_{drop}^{0.44}$, which for constant interfacial tension is in reasonable agreement with results for low capillary-number flows[36] of $W \propto V_{drop}^{0.5}$. Therefore, drops can be merged and their contents mixed at predictable – and controllable – points in space (cm to meters) and time (seconds to days) by starting and stopping the syringe pump. The effects of gravity are mitigated by positioning tubes horizontally. We were unable to detect any change in drop size due to evaporation over several days. For conditions yielding different capillary numbers, different excess velocities will apply.

Many drops may be merged using trains with multiple aqueous drops; however the relative velocity of all drops needs to be known in order to predict where and when drops merge. Figure 5 illustrates how the excess velocity of drops 2-10 relative to drop 1 can be determined in trains with 10 drops (the first drop has an excess velocity of zero). When the separating oil contains surfactant, the velocity of each drop is dependent on its relative position in the train, which increases with drop position from the front. The cause of this increase is believed to be due to a continuously-varying surfactant concentration along each aqueous drop due to transport of surfactants around the drop interface. [The surfactant is attracted to the water interface due to the hydrophilic head group.] Internal circulation within the drop[38] then transfers surfactant from front to rear, whence it is transferred to the next separating compartment. Therefore, flow transforms an initially homogenous separating fluid into one that increases in surfactant concentration from the first to last separating compartment.

Consequently, the surfactant concentration of each drop varies with flow, and the interfacial tension (and hence Capillary number and excess velocity) is dynamic from two perspectives. Within each drop, circulation continuously redistributes surfactant along the interface of that drop; between drops, surfactant is transferred down the train. Such redistribution is evident from an increased turbidity of last separating compartment (as confirmed in Fig. 6B) – presumably due to micelle accumulation.

The distribution of drop velocities in Figure 5 suggests that velocity variations between successive drops will increase/decrease as surfactant concentrations in the separating fluid decrease/increase, and that saturation of the interface with surfactant will eventually limit the scale of the change. To confirm this, surfactant-free fluids were used to create trains with 10 aqueous drops. For the surfactant-free case (Fig. 5, black bars), the velocity of each drop remained constant irrespective of position in the train. This result points to future work where these fluidic architectures are used to filter or concentrate molecules of interest (as done with surfactant here).

Based on measurements like those described above, surfactant-free fluids enable merging in sequential order from first to last irrespective of droplet spacing. However, when using surfactant within the separating fluid, drop-to-drop spacing may need to be altered to account for variation in relative drop velocity. By way of example, consider the 10-drop train and surfactant-laden separating fluid data of Figure 5. At one meter from the tube inlet, the distance between drop 1 and 2 reduces by 11 mm, while the distance between drop 1 and 3 reduces by 11.7 mm. Therefore, if the initial spacing between drops 2 and 3 was less than 0.7 mm, drops 2 and 3 would merge before drops 1 and 2. By controlling inter-drop distance and flow rates (and possibly the surfactant concentration in separating compartments), it is conceivable that trains can be designed where drops can be merged in any desired sequence.

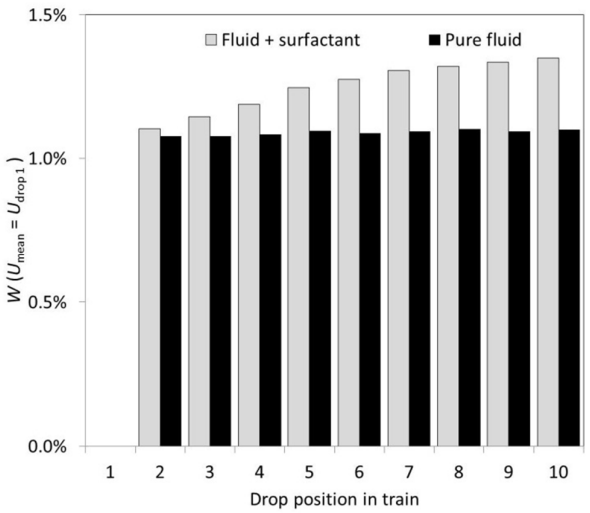

Figure 5. Velocity excess of each drop relative to the leading drop in a 10-drop train (350-µm tube; carrier-fluid velocity 5.8 mm/s). Grey bars: fluids – HFE 7500, water + dye, tetradecane + 1% Span80. Black bars: fluids – FC40, water + dye, 5 cSt silicone oil.

We next demonstrate the sequential and ordered merging of 51 water drops one after another to give a single enlarged one using the architecture shown in Figure 6A. Here, a robot controls tube dipping. As each drop passes LED1, the voltage peaks (blue voltage trace in Figure 6A). As the train travels towards LED2, drop 2 merges with drop 1, then drop 3 with the now-enlarged leading water drop, and so on until all drops merge successively into one giant drop (red voltage trace in Figure 6A).

Thus far, we have mainly considered merging drops in one train. More drops can be merged using more trains (in series) and tubes (in parallel). In Figure 6B and Movie S2, four 1.35-m long tubes are attached to 4 syringes driven by one pump, and a robot dips tube ends into appropriate fluids to generate a series of trains. Such dipping has been used previously,[39] but then the tube tip passed directly from one aqueous reagent to another, and this could result in cross-contamination (see below). Each train contains two water drops carrying dye of the same colour, and drops have volumes of 40 and 60 nl; successive trains carry differently-coloured dyes. Flow again induces drops to merge, with drops of the same contents (colour) merging at approximately the same locations. The pairs of red and blue drops merge at slightly different points; this is due to the different dyes altering the interfacial tension of the water to slightly different degrees. This can be seen in greater detail in an analogous experiment illustrated in Figure S2 (which involves the merging of pairs of drops in 206 trains). Figure S3 also shows selected trains in a second tube with different contents run in parallel to the one illustrated in Figure S2. As the pump used can drive 10 syringes, drops in ~1,000 completely different trains can be prepared and mixed in ~15 min in this way (as in Movie S3).

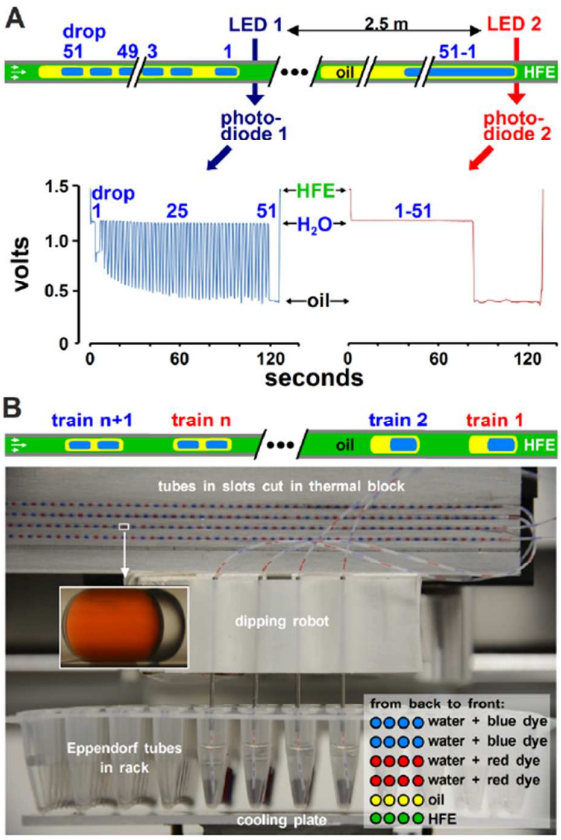

Figure 6. Multiplexed merging. (A) Merging 51 drops in one train (620-µm tube; fluids – HFE7500, water, tetradecane + 2.5% Span80). Photo-diode voltage reflects which fluid is in the light beam. Fifty-one 800-nl aqueous drops are engulfed in one oil super-drop; this train passes through the first light beam to yield the blue voltage trace. Voltage levels confirm that an oil super-drop engulfs 51 water drops (the space between drops 1 and 2 is greater than the others). Once the last of the oil passes LED1, drops merge one after another, and pass LED2 to yield the red voltage trace (which confirms all water drops have merged). A stereoscope was used to visually confirm that each drop was added to the enlarging first drop in their numerical order. (B) Merging hundreds of drop pairs in many trains (fluids – 75% FC40 + 25% HFE7500, water + red or blue dye, tetradecane + 1% Span80). Four bipartite tubes – made by joining 250- and 460-µm bore tubes (used for drop merging and storage, respectively) – are each attached to syringes driven by one pump (out of sight at top left); the other ends of the 4 tubes are dipped by a robot successively into appropriate fluids in Eppendorf tubes (arrangement shown at bottom right) on the cooling plate (not used here) to generate a series of trains (each with two 50-nl water drops + dye of the same color, as in the schematic above). Successive trains carry differently-colored dyes. Flow induces drops to merge by the time trains reach the thermal block (not used here; inset – magnification of merged drop). The number of drops that can be merged like this is limited only by fluid volume, syringe capacity, and tube length. See also Movie S2.

Transferring fluid between drops through nano-channels

A challenge in microfluidics is delivering reagents to drops with temporal control, which can be achieved by molecular diffusion through walls[19,20] – but then control depends on wall porosity. Our system provides a simple way of transferring cargoes of interest. The two internal phases in Figure 1B are inverted when $\gamma_{1\text{-}3} > \gamma_{1\text{-}2} + \gamma_{2\text{-}3}$. This is achieved in Figure 7Ai using FC40 + 10% PFO (1H,1H,2H,2H perfluoro-1-octanol;

phase 1), 1% TritonX100 in water (phase 2), and dodecane (phase 3). Here, an air drop restrains train speed, as air has the highest interfacial tension with FC40[37] and hence the lowest velocity. During flow, the oil drop (initially engulfed in aqueous drop 2) soon catches up aqueous drop 1 (Fig. 7Aii), and the two water drops merge. The resulting super-drop contains aqueous sub-compartments 1 and 2 connected by channels ("thin liquid films") around the oil. As flow continues, the oil drop continues to catch up the front of the super-drop; consequently, water flows back through the channels (Figure 7Aiii,iv; Movies S4 and S5). Rates of such advection (range fl/s – µl/s) depend on the velocity of the oil drop relative to the engulfing water drop – which is proportional to Capillary number (see Figure 4B).[36] Consequently, rates can be altered by varying tube diameter and/or Capillary number. When flow stops, there is little diffusional transfer between compartments as the aqueous channels are so long.

Discrete volumes can be delivered stepwise by such advection. Using the initial architecture in Figure 7Bi, flow backwards causes the oil drop to catch up the aqueous drop, creating an aqueous super-drop containing fluorescein (F) in one compartment and water in the other (Figure 7Bii). [At this stage, no fluorescein is detected in drop 2, so there is no net fluid flow from compartment F to 2. However for a non-circular channel this may not be the case, as it has been shown that a drop can travel faster or slower than the mean carrier-fluid velocity depending on surfactant levels.[40,41]] In our case when flow is reversed, fluorescein is carried through the connecting channels (Figure 7Biii). Now flow is again reversed for 60 s to mix the contents of 2 as it travels ~3 compartment lengths (Figure 7Biv). [This induces some fluorescein flow from 2 back to F, but relatively little is transferred because of prior dilution in the large volume of 2.] Cycles of 5-s flow in one direction and 60-s in the other deliver 2.5-pl aliquots of fluorescein (at ~500 fl/s) to compartment 2, and then mixes contents (Figure 7Bv). Even smaller aliquots can be delivered by reducing flow rates or increasing the interfacial tension (both altering the Capillary number) and/or varying tube diameter. Here, the connecting channel is a ring ~40 nm wide separating the oil and fluorocarbon. [The scale of the ring is calculated assuming $viscosity_{oil}$ >> $viscosity_{water}$, (in the other limit where $viscosity_{oil}$ << $viscosity_{water}$, film thickness would be expected to be half this value; see Experimental section).[35]] As ring width can be varied by changing tube diameter and *Ca*, this suggests that such nano-channels can be used to filter particles in this size range.

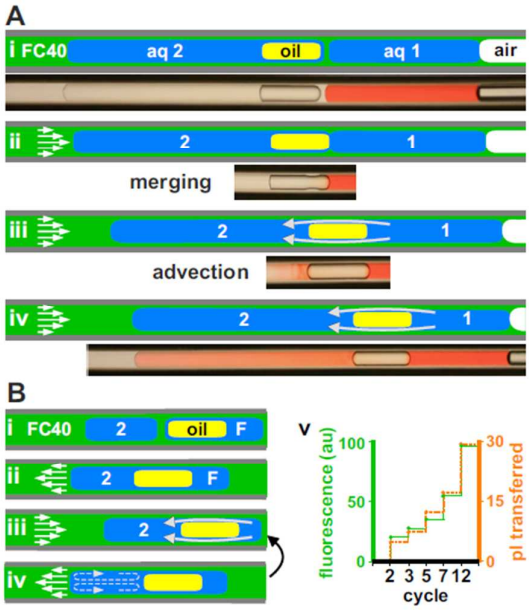

Figure 7. Transferring fluids between compartments through nano-channels (fluids – FC40 + 10% PFO, 1% TritonX100 in water ± red dye, oil indicated). (A) Example (150-µm tube). Schematics illustrate structures seen in movie frames below. (i) Train: air drop, 20-nl drop 1 + red dye, aqueous super-drop 2 engulfing a dodecane drop. (ii) On flow (white arrows), the oil catches up 1, and 2 merges with 1; now, an aqueous channel (a ring around the oil) connects 2 with 1. (iii,iv) Oil advances; water flow (~300 pl/s) carries dye back from 1 to 2 (grey arrows). (B) Advection rates (50-µm tube). (i) Train: a 1.5-nl aqueous super-drop + carboxy-fluorescein (F) engulfs a 2-nl sunflower-oil drop, 2.5-nl water-drop 2. (ii) During flow to left, the oil catches up 2, drops merge, and aqueous channels now connect F to 2. (iii) Flow is reversed; advection (~500 fl/s; grey arrows) carries dye from F to 2. (iv) Reversing flow as 2 traverses three compartment-lengths and mixes contents (dashed grey arrows). A fluorescence micrograph is collected, before cycles iii to iv repeat (black arrow). (v) Fluorescence intensity (arbitrary units, au) in drop 2 after cycle number indicated (fl transferred calculated from shrinkage rate of F).

Cross-contamination

Although most bio-molecules are insoluble in fluorocarbons and oils, some might nevertheless diffuse between drops and/or adhere to walls and then dissociate to contaminate the next drop or train as it passes. Contamination could also occur when making a train with progressively more and more aqueous drops so the protecting fluorocarbon layer abutting the wall becomes so thin it eventually disappears (e.g., when making trains with more aqueous drops than in Fig. 6A). Then, only separating fluid would provide a barrier between the aqueous drops and the wall. [In such a case, the potential for cross contamination would be similar to that obtained with most existing two-phase microfluidic droplet-based networks.] Therefore, we assessed the level of such cross-contamination by monitoring the unwanted transfer of fluorescein or DNA (using sensitive fluorescence or PCR-based assays; Figs S3 and S4). Such experiments showed that if cross-contamination did occur, it did so at a level that can be neglected when carrying out the proof-of-principle applications now described.

Two applications

Crystallizing proteins

Finding conditions permitting protein crystallization represent major bottlenecks in determining tertiary structure by X-ray crystallography. Crystals are usually obtained by screening different protein/precipitant concentrations to find ones suitable for crystal growth, and – because protein supply is often limited – microfluidic devices are sometimes used.[42] Here, we use lysozyme (L) as an example (Fig. 8). Serial protein dilutions are made using a train containing lysozyme in the first aqueous drop and precipitant in drops 2-6. Flow both generates one aqueous super-drop separated by oil drops into sub-compartments, and drives advection that carries protein back through the connecting nano-channels to create serial dilutions. After stopping the train, crystals form in compartments containing appropriate conditions. Here a water-based surfactant was added to carrier (and not water), so commercially-available preparations of precipitant could be used as supplied.

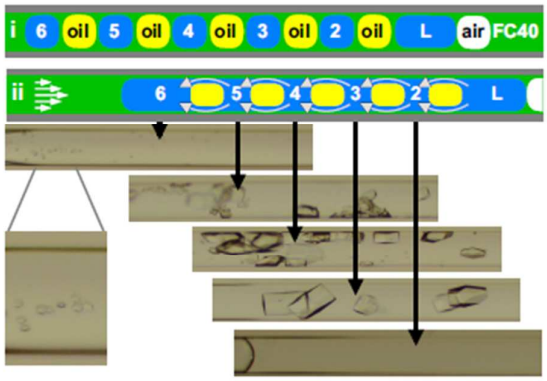

Figure 8. Screening crystallization conditions (150-µm tubes; fluids – FC40 + 5% PFO + 1% TritonX100, aqueous phase, tetradecane; schematics not to same scale as micrographs below). (i) Train: air drop to control train speed, water drop 1 (60 nl) contains lysozyme (L), and drops 2-6 (20 nl) precipitant. (ii) Flow (straight arrows) creates an aqueous super-drop engulfing 5 oil drops, and drives advection between compartments (curved arrows) to create a gradient in protein concentration. After stopping flow and incubation (3 h), micrographs of compartments 2-6 are shown.

Screening drugs for effects on human cells

Screening scarce chemicals to see which might serve as useful drugs represents an attractive application for microfluidics. Therefore, we first screened fluids to see which might allow human cells to survive in drops-in-drops, and found suitable ones (using a threshold of >90% survival after 24 h, assessed using trypan-blue exclusion). As proof-of-concept, we compared the effects of mixing various drugs with cells grown conventionally in plates or in drops (using the fluidic architecture in Fig. 9A) – and obtained similar results.

For example, tumor necrosis factor α (TNFα) is a pro-inflammatory cytokine that can switch on expression of the green fluorescent protein (GFP) in a Jurkat line encoding a GFP-reporter gene under the control of a responsive promoter. This line is derived from a T lymphocyte and grows in suspension. When imaged in a tube under ultra-violet light, untreated cells are non-fluorescent; however, cells treated with TNFα for 20 h fluoresce green (Fig. 9Bi). When cells from similar trains are ejected from tubes and passed through a FACS (fluorescence activated cell sorter), intensities are found to be ~100-fold greater than those given by untreated cells; they are also similar to those in cells grown conventionally (Fig. 9Bii). TNFα had much the same effect when added to human embryonic kidney cells growing on the surface of dextran beads and which encoded a related GFP-reporter gene (Fig. S5A,B). This demonstrates that our approach can be used with both suspension and adherent cells.

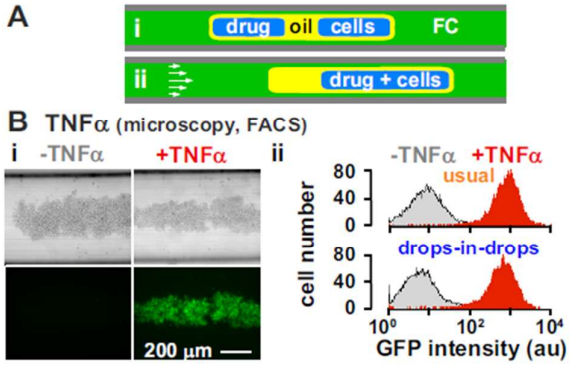

Figure 9. Drug screening: proof-of-principle. (A) Approach (FC is a mixture of fluorocarbons). (i,ii) Flow delivers drug to cells. (B) TNFα induces GFP expression in (initially non-fluorescent) NF-κB/Jurkat/GFP™ Reporter cells (560-µm tubes; fluids – 50% FC40 + 50% HFE7500, cells in growth medium ± TNFα, 5-cSt silicone oil + 0.25% AbilEM180). After merging delivers drug, tubes were incubated (37°C; 20 h). (i) Bright-field and fluorescence images of tubes containing cells treated ± TNFα (20 h). (ii) Cells were ejected from similar tubes, and GFP-intensities (au, arbitrary units) seen in 10^4 cells analyzed using FACS. Cells grown conventionally in plates ("usual") provide controls.

The use of various other cell/drug combinations and readouts confirmed the potential of our device for drug screening; in all cases, cells in tubes behaved like their counterparts grown conventionally. For example: (i) TNFα increases levels of TNFAIP2 mRNA in HeLa cells growing on the surface of dextran beads (Fig. S5C).[43] (ii) DRB (5,6-dichloro-1-β-D-ribo-furanosyl-benzimidazole) – a protein kinase inhibitor that blocks elongation by RNA polymerase II – reduced levels of c-MYC mRNA in Jurkat cells in suspension (assessed using quantitative reverse-transcriptase PCR, qRT-PCR; Fig. S6A,B). (iii) Using the same cells, ionomycin plus PMA (phorbol 12-myristate 13-acetate) – a stimulant – increased those of IL2 mRNA (assessed using RT-PCR; Fig. S6C).[44] These results (obtained using different human cells growing in suspension or attached to surfaces, and both activators and inhibitors) – together with the multiplexing described earlier – provide proof-of-principle demonstrations that our device could be used for drug screening. They also confirm its versatility and biocompatibility.

Conclusions

In summary, by exploiting interfacial tension and at least three immiscible fluids we have demonstrated a novel approach to enable the controlled coalescence of many drops. Using the same physical principle, we also demonstrate a new method for controlled transport of media through nano-channels between many drops. These new approaches for merging drops and advection between them are achieved using a single Teflon tube with no surface modification, and manual drop loading. Consequently, they can be replicated without requirement for a dedicated microfluidics laboratory. As many drops and trains can be created using a robot, manipulations are also scalable. By selecting appropriate fluids, we have demonstrated biocompatibility through two proof-of-concept applications – protein crystallisation and screening drugs for their effects on human cells growing in suspension or on surfaces. These novel approaches should find many other applications where small volumes of fluids are manipulated.

Acknowledgements

We thank Oreste Acuto for Jurkat cells, and the Medical Research Council (AF, PRC), the Indonesian Endowment Fund for Education (AP), the 7th Framework Marie Curie Career Integration grant contract No. 333848, and University of Oxford John Fell Fund (EW) for support.

Notes and references

1 N. Wu, Y. Zhu, S. Brown, J. Oakeshott, T. S. Peat, R. Surjadi, C. Easton, P. W. Leech and B. A. Sexton, *Lab on a Chip*, 2009, **9**, 3391-3398.
2 M. R. Bennett and J. Hasty, *Nat. Rev. Genet.*, 2009, **10**, 628-638.
3 A. K. White, M. VanInsberghe, O. I. Petriv, M. Hamidi, D. Sikorski, M. A. Marra, J. Piret, S. Aparicio and C. L. Hansen, *PNAS*, 2011, **108**, 13999-14004.
4 C. M. Hindson, J. R. Chevillet, H. A. Briggs, E. N. Gallichotte, I. K. Ruf, B. J. Hindson, R. L. Vessella and M. Tewari, *Nat. Meth.*, 2013, **10**, 1003-1005.
5 R. Williams, S. G. Peisajovich, O. J. Miller, S. Magdassi, D. S. Tawfik and A. D. Griffiths, *Nat. Meth.*, 2006, **3**, 545-550.
6 P. H. Hoang, H. Park and D. P. Kim, *J. Amer. Chem. Soc.*, 2011, **133**, 14765-14770.
7 P. C. Blainey, *FEMS Microbio. Rev.*, 2013, **37**, 407-427.
8 A. Fallah-Araghi, J. C. Baret, M. Ryckelynck and A. D. Griffiths, *Lab on a Chip*, 2012, **12**, 882-891.
9 N. Bremond, A. R. Thiam and J. Bibette, *Phys. Rev. Lett.*, 2008, **100**, 024501.
10 D. J. Eastburn, A. Sciambi and A. R. Abate, *Plos One*, 2013, **8**.
11 S. Q. Gu, Y. X. Zhang, Y. Zhu, W. B. Du, B. Yao and Q. Fang, *Analytical Chemistry*, 2011, **83**, 7570-7576.
12 J. Q. Boedicker, L. Li, T. R. Kline and R. F. Ismagilov, *Lab on a Chip*, 2008, **8**, 1265-1272.
13 J. Hong, M. Choi, A. J. deMello and J. B. Edel, *BIOCHIP JOURNAL*, 2009, **3**, 203-207.
14 I. Akartuna, D. M. Aubrecht, T. E. Kodger and D. A. Weitz, *Lab on a Chip*, 2015, **15**, 1140-1144.
15 N. N. Deng, J. Sun, W. Wang, X. J. Ju, R. Xie and L. Y. Chu, *Acs Appl Mater Inter*, 2014, **6**, 3817-3821.
16 L. Baraban, F. Bertholle, M. L. M. Salverda, N. Bremond, P. Panizza, J. Baudry, J. A. G. M. de Visser and J. Bibette, *Lab on a Chip*, 2011, **11**, 4057-4062.
17 V. Trivedi, A. Doshi, G. K. Kurup, E. Ereifej, P. J. Vandevord and A. S. Basu, *Lab on a Chip*, 2010, **10**, 2433-2442.
18 Y. Zhu, Y. X. Zhang, W. W. Liu, Y. Ma, Q. Fang and B. Yao, *Sci Rep-Uk*, 2015, **5**.
19 F. Courtois, L. F. Olguin, G. Whyte, A. B. Theberge, W. T. S. Huck, F. Hollfelder and C. Abell, *Anal. Chem.*, 2009, **81**, 3008-3016.
20 J. Shim, S. N. Patil, J. T. Hodgkinson, S. D. Bowden, D. R. Spring, M. Welch, W. T. S. Huck, F. Hollfelder and C. Abell, *Lab on a Chip*, 2011, **11**, 1132-1137.
21 Liang-Yin Chu, Andrew S. Utada, Rhutesh K. Shah, Jin-Woong Kim and D. A. Weitz, *Angew. Chem. Int. Ed.*, 2007, **46**, 8970-8974.
22 A. R. Abate and D. A. Weitz, *Lab on a Chip*, 2011, **11**, 1911-1915.
23 N. Wu, J. G. Oakeshott, C. J. Easton, T. S. Peat, R. Surjadi and Y. Zhu, *J Micromech Microeng*, 2011, **21**, 1-7.
24 R. K. Shah, H. C. Shum, A. C. Rowat, D. Lee, J. J. Agresti, A. S. Utada, L. Y. Chu, J. W. Kim, A. Fernandez-Nieves, C. J. Martinez and D. A. Weitz, *Mater Today*, 2008, **11**, 18-27.
25 C. X. Zhao, *Adv Drug Deliver Rev*, 2013, **65**, 1420-1446.
26 E. Q. Li, J. M. Zhang and S. T. Thoroddsen, *J Micromech Microeng*, 2014, **24**.
27 J. Rowlinson, ed., *Molecular Theory of Capillarity*, Clarendon Press Oxford, 1982.
28 J. Guzowski, P. M. Korczyk, S. Jakiela and P. Garstecki, *Soft Matter*, 2012, **8**, 7269-7278.
29 J. Guzowski and P. Garstecki, *Lab on a Chip*, 2014, **14**, 1477-1478.
30 J. D. Tice, H. Song, A. D. Lyon and R. F. Ismagilov, *Langmuir*, 2003, **19**, 9127-9133.
31 C. King, E. Walsh and R. Grimes, *Microfluidics and Nanofluidics*, 2007, **3**, 463-472.
32 D. L. L. Chen, L. Li, S. Reyes, D. N. Adamson and R. F. Ismagilov, *Langmuir*, 2007, **23**, 2255-2260.
33 J. A. Howard and P. A. Walsh, *Inter. J. Multiphase flows*, 2013, **55**, 32-42.
34 P. Aussillous and D. Quere, *Physics of Fluids*, 2000, **12**, 2367-2371.
35 M. E. Charles, *Can. J. Chem. Eng.*, 1963, **41**, 46-51.
36 F. Fairbrother and A. E. Stubbs, *J. Chem. Soc.*, 1935, 527-529.
37 F. P. Bretherton, *J. Fluid Mech.*, 1961, **10**, 166-188.
38 J. Ratulowski and H. C. Chang, *Journal of Fluid Mechanics*, 1990, **210**, 303-328.
39 W. B. Du, M. Sun, S. Q. Gu, Y. Zhu and Q. Fang, *Anal. Chem.*, 2010, **82**, 9941-9947.
40 M. J. Fuerstman, A. Lai, M. E. Thurlow, S. S. Shevkoplyas, H. A. Stone and G. M. Whitesides, *Lab on a Chip*, 2007, **7**, 1479-1489.
41 J. C. Baret, *Lab on a Chip*, 2012, **12**, 422-433.
42 L. Li, Q. Fu, C. A. Kors, L. Stewart, P. Nollert, P. D. Laible and R. F. Ismagilov, *Microfluid Nanofluid*, 2010, **8**, 789-798.
43 A. Papantonis, T. Kohro, S. Baboo, J. Larkin, B. Deng, P. Short, T. Tsutsumi, S. Taylor, Y. Kanki, M. Kobayashi, G. Li, H.-M. Poh, X. Ruan, H. Aburatani, Y. Ruan, T. Kodama, Y. Wada and P. R. Cook, *J. EMBO*, 2012, **31**, 4404-4414.
44 E. M. Schwarz, P. Salgame and B. R. Bloom, *P. Nat. Acad. Sci. USA*, 1993, **90**, 7734-7738.